Numerical and Experimental Modeling of Natural Convection for a Cryogenic Prototype of a Titan Montgolfiere

Yu. Feldman[1] and T. Colonius[2]
California Institute of Technology, Pasadena, Ca, 91125, USA

and

M. Pauken[3] , J. L. Hall[4] and J. A. Jones[5]
Jet Propulsion Laboratory, California Institute of Technology, Pasadena, Ca, 91109, USA

Natural convection in a spherical geometry is considered for prediction of the buoyancy characteristics of one meter diameter single- and double-walled balloons in a cryogenic environment. The steady-state flow characteristics obtained by solving the Reynolds-Averaged Navier Stokes equations (RANS) with a standard k-ε model are used to determine the balloon performance in terms of net buoyancy as a function of heat input. Thermal radiation effects on the overall balloon performance are also investigated. The results obtained compared favorably with the corresponding cryogenic experiments conducted at the same scale in a cryogenic facility. In addition, both numerical and experimental results were compared with engineering heat transfer correlations used in system-level models of the Titan Montgolfiere. Finally, we examine scaling issues for the full-scale Titan Montgolfieres.

Nomenclature

B	=	buoyancy
C	=	constant in Sutherland's law
D	=	diameter
g	=	gravitation acceleration
h	=	convection coefficient
k	=	thermal conductivity
L	=	gap width
M	=	Molar mass
Nu	=	Nusselt number

[1] Postdoctoral Scholar, Mechanical Engineering. Member AIAA.
[2] Professor, Division of Engineering and Applied Science. Associate Fellow AIAA.
[3] Senior Engineer, Fluid and Thermal Systems. Senior Member AIAA.
[4] Senior Engineer, Mobility and Robotic Systems. Senior Member AIAA.
[5] Principal Engineer, Advanced Technology. Member AIAA.

Pr = Prandtl number

$\dot{Q}$ = power input

R = universal gas constant

Ra = Rayleigh number

Ra^* = modified Rayleigh number

T = temperature

ε = surface emissivity

ξ = relative deviation between measurements

μ = dynamic viscosity

σ = Stefan-Boltzman constant

ρ = density

ϕ = ratio of inner and outer diameters

Subscripts

b = balloon

eff = effective

exp = experiment

ext = external

g = gap

i = inner

int = internal

o = outer

rad = radiation

sim = simulation

I. Introduction

DESPITE vast differences in environmental conditions, Saturn's moon Titan is thought to look more like the Earth than any other body in the solar system. It is believed that Titan hosts chemistry similar to pre-biotic conditions on Earth. Its thick and cold atmosphere is comprised mostly of nitrogen. Low gravity (one-seventh of Earth) and temperature together make a hot air balloon (or Montgolfiere) an attractive configuration for a Titan aerobot. In contrast to the terrestrial Montgolfieres for which the majority of heat is lost by thermal radiation, the Tittan Montgolfiere will be dominated by convective heat transfer. These factors imply that relatively moderate power of about 2 kW may be sufficient for certain scientific missions [1]. An extensive study discussing pros and cons of various aerial platforms for a long endurance survey of Titan surface can be found in the recent work of Dorrington [2].

Computational fluid dynamics (CFD) is a power tool for numerical prediction and optimization of the hot balloon's thermal characteristics. For the full-scale Montgolfiere, three-dimensional analysis that fully resolves the

unsteady, turbulent convection is unfeasible because of the CPU requirements, but simplified calculations can be performed by employing turbulence models (i.e. modeling the time-averaged flow) for an axi-symmetric geometry. However, such calculations require an extensive validation study with experimental results. For experiments in the terrestrial environment, it is not possible to achieve full similarity with a proposed Titanic mission [3], and compromises must therefore be made between sub-scale experiments at cryogenic conditions, and full-scale testing at normal temperatures. For the latter case, thermal radiation losses must also be carefully estimated and isolated in order to translate the results to cryogenic conditions.

In our previous study [1], computational models predicting the natural convection heat transfer and buoyancy for a cryogenic Titan Montgolfiere were developed. The CFD models demonstrated reasonable agreement with limited experimental data, and revealed some limitations of idealized engineering correlations, which tended to over-predict buoyancy in comparison with experimental and numerical results. The thermal radiation effect was not addressed. The results motivated our present research aimed at generating more refined CFD models and experimental data for evaluating engineering correlation models. The present paper reports on this ongoing effort and is organized as follows. Section II describes the experimental set up and methodology. Section III details the basic assumptions of the numerical simulations. Section IV describes semi-analytical heat transfer calculations based on the engineering correlations. Section V presents an extensive discussion of the results, and conclusions are placed in section VI.

II. Experimental Setup

Two prototype balloons were tested at cryogenic temperatures covering the temperature range found in Titan's atmosphere. Each balloon had a nominal diameter of 1 m. One balloon had a single wall, while the second balloon had a double wall with a 5 cm gap between the inner and outer walls, or $\phi = D_i / D_o = 0.9$. The balloons were made buoyant by electrically heating the gas. Voltage and current measurements on the heater allows for an accurate measure of the heat input necessary for calculating the energy balance on the balloon. The balloons were instrumented with thermocouples embedded within the walls to measure skin temperature at several locations from crown to base. The gas temperature inside the balloons was measured in two locations. One location was along the vertical centerline above the electrical heater and the other location was along the equator mid-way between the heater and the balloon skin. The balloons were anchored to a load cell to measure the net lift of the balloons. The load cell was placed inside a heated and insulated container to ensure the unit remained close to room temperature during the test.

A schematic of the cryogenic test facility is shown in Fig. 1. The cryogenic chamber sprays liquid nitrogen through a circulation fan within the chamber. A steel cylindrical shell was placed within the cryogenic chamber to provide a "quiet" atmosphere around the balloon during testing. Thermocouples were placed on a grid inside the cylindrical shell to measure the gas temperature around the balloon. The temperature of the cylindrical shell wall was also measured since it provides a boundary condition for the test set up. Two cameras and several lights were located within the cylindrical shell to observe and record the behavior of the balloon during the test. A screen shot of the double wall balloon inside the chamber from the down-looking camera is shown in Fig 2. It was noted during the testing, that the balloons tended to oscillate slowly. This oscillation was probably a result of convection currents

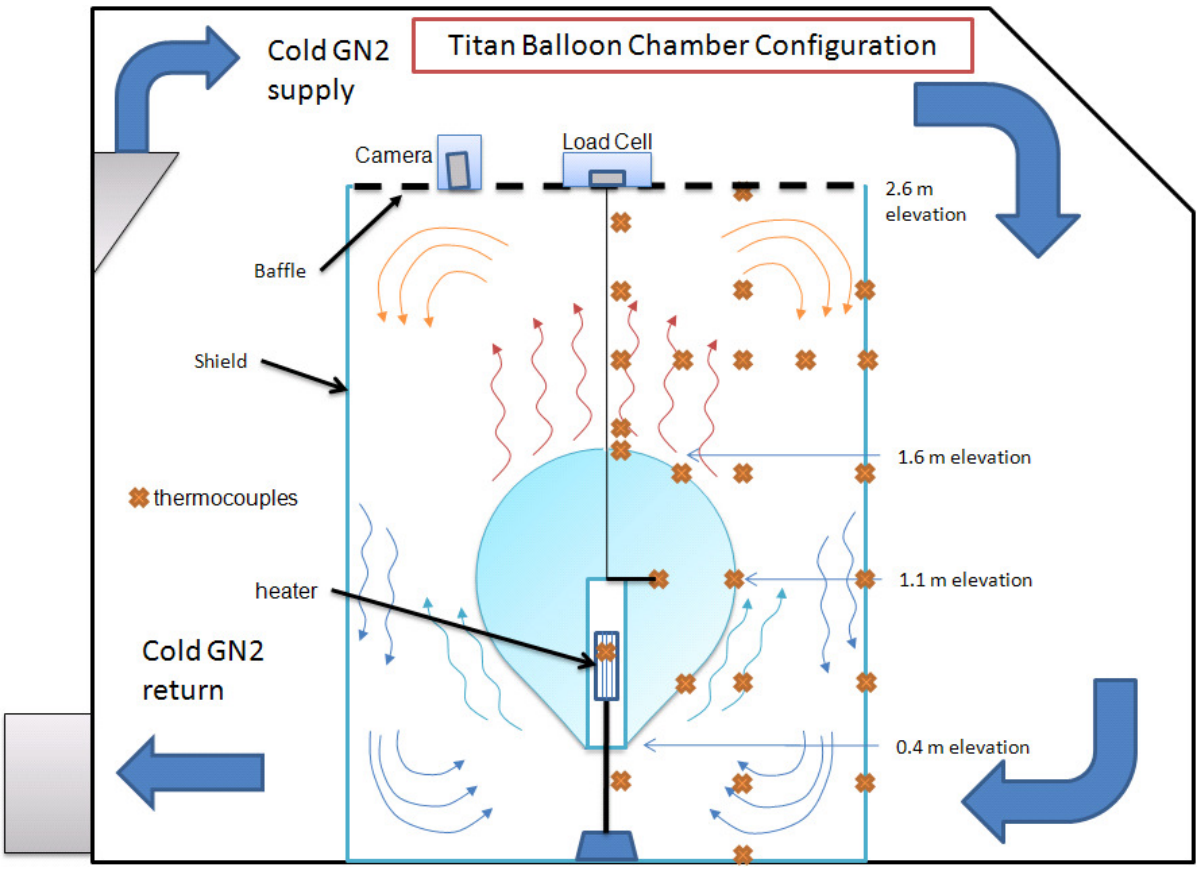

Figure 1. A schematic description of experimental setup for a single-walled balloon.

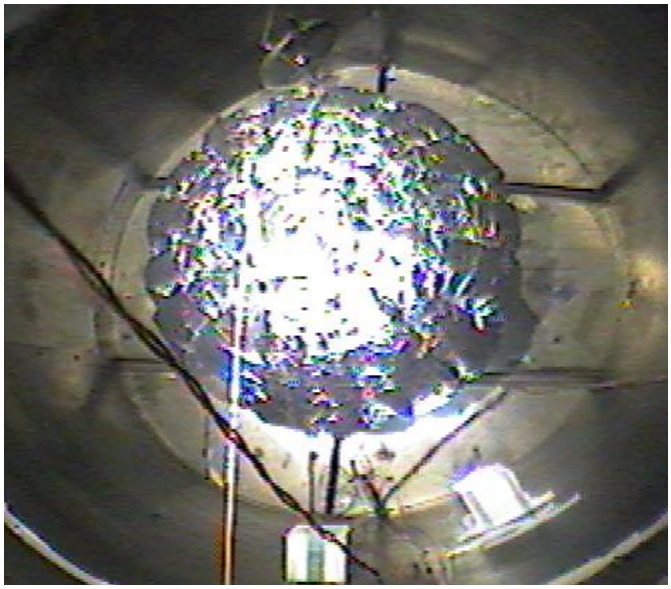

Figure 2. Double-walled balloon floating in the cryogenic chamber.

circulating within the shell due to the cold shell walls and the warm balloon skin. Testing each balloon first required heating them at ambient conditions to make them buoyant. Once the balloon was inflated, the cylindrical shell surrounding the balloon was closed. The cryogenic chamber was also closed and cooling was started. The balloon heater power was reduced to the lowest heater set point during the cool-down period. (Heat input required for buoyancy at ambient conditions is significantly greater than the power required at cryogenic temperatures). After the chamber reached its first operating temperature the heat input to the balloon was stepped through different power levels until equilibrium conditions were obtained for several different settings of heater power level. In some cases redundant measurements were made by reducing heater power after reaching the highest level to check for repeatability or hysteresis. Equilibrium conditions were assumed to be achieved when the chamber temperature was maintained within ± 5 K of the target set point, and internal temperatures varied less than ±1 K over a 10 minute period. Fluctuations in buoyancy were less than 5% over the same period. After all power level settings had been tested, the balloons were tested at a second environment temperature by lowering the chamber temperature again, and completing another series of measurements for each power level. The various equilibrium conditions achieved for both balloons are listed in Table 1.

Table 1. List of equilibrium conditions checked in experiments.

Single-walled balloon, $\dot{Q}$[W]					
T_∞= 90K	103	254	407	549	
T_∞= 140K		252	402	553	
T_∞= 180K		251	399	552	
Double-walled balloon, $\dot{Q}$[W]					
T_∞= 90K	103	254	411	546	700
T_∞= 140K		266	410	550	

The balloons had a sphere-on-cone shape and the actual volumes and surface areas differed from the assumed spheres of 1 m O.D. In particular, the single-walled balloon had a surface area and volume that were 3 and 7% smaller than the sphere, respectively. For the double-walled balloon these were 10% and 15%, respectively. In addition, it was observed that for the double-walled balloon, full inflation was not achieved at some of the lower heat inputs.

III. Numerical Simulation

Numerical simulations of the turbulent, free convection were computed for both single- and double-walled balloons using commercial CFD software, Ansys 13. As a first approximation, we modeled the balloon as a spherical shell (or a pair of concentric shells), contained in a rigid, uniform temperature cylinder of the same dimensions of the shield employed in the experiments. We choose the inner and outer diameters of the shells to be 1 m and 0.9 m respectively which is acceptable approximation for the realistic geometry of the balloons used in the experiment.

The time-averaged turbulent flow is expected to be axisymmetric, which results in substantially reduced run times compared to a 3D model. The heat source was idealized compared to the actual strip heater in the experiments,

in that we neglect the presence of fins, and specify a uniform heat flux, per unit area, on the cylindrical surface of height 0.1524 m and radius 0.0508 m . The idealization allowed us to investigate the influence of surface radiation effects on the balloon's thermal efficiency. A surface to surface radiation model (S2S) was utilized for this purpose, and accounts for the mutual radiation heat transfer from all boundaries. The balloon material was aluminized Mylar with the emissivity values equal to $\varepsilon = 0.04$ and $\varepsilon = 0.28$ for the balloon/gap internal and external surfaces respectively. The emissivity value of the heat source was estimated to be $\varepsilon = 0.28$. The balloon surfaces are assumed to be perfectly conducting (negligible thickness) such that the same temperature exists on both sides of the boundary at a given location.

We employed the Boussinesq approximation of incompressible buoyancy driven flow. The approximation of incompressible flow is reasonable in the present case where the characteristic buoyancy-induced velocities are no more than 2 m/s. We note that a more restrictive Boussinesq approximation also assumes that temperature differences are small compared to ambient temperature, so that $(T\text{-}T_\infty)/T_\infty \ll 1$ and consequently,

$$\rho = \rho_\infty(1 - (T - T_\infty)/T_\infty). \tag{1}$$

This assumption was made in our previous modeling efforts and considerably simplifies numerical model [1]. While this approximation is likely very reasonable for a full-scale Titan Montgolfiere (where temperature differences are relatively low), for the present (roughly 1/10th-scale) model, $(T\text{-}T_\infty)/T_\infty$ may reach values as high as 0.43. In the present study, we therefore relaxed the second assumption and instead used the ideal gas law, simplified under the first Boussinesq approximation,

$$\rho = P_\infty M/RT, \tag{2}$$

where P_∞ is the ambient pressure, M is the nitrogen molar mass and R is the universal gas constant. At the same time the nitrogen local viscosity μ, and local thermal conductivity k are obtained by Sutherland's law

$$\mu = \left(\frac{T}{T_0}\right)^{1.5} \mu_0(T_0 + C)/(T + C),\ T_0 = 300.55,\ \mu_0 = 17.81 \times 10^{-6}, C = 111, \tag{3}$$

$$k = \left(\frac{T}{T_0}\right)^{1.5} k_0(T_0 + C)/(T + C), T_0 = 300.55,\ k_0 = 0.02604, C = 111. \tag{4}$$

The temperature dependency of the nitrogen specific heat values c_p was addressed by using its tabulated values. Once simulations converged to steady-state conditions, the net buoyancy B was evaluated as

$$B = \int(\rho_\infty - \rho)\, g dV, \tag{5}$$

where the densities were evaluated from temperatures according to Eq. (2).

For the range of Rayleigh numbers achieved in the experiments, one expects fully turbulent natural convection, including thin natural convection boundary layers on the surfaces and free turbulence in the buoyant plumes rising from the heat source and the crown of the balloon. For the turbulence, we used a standard $k\text{-}\varepsilon$ model [4] allowing for determination of turbulent velocity and length scales by solving two additional transport equations for kinetic energy k and dissipation rate ε. Standard wall functions were used to resolve turbulent boundary layers at all surfaces. The spatial discretizatization was implemented by a second order upwind scheme.

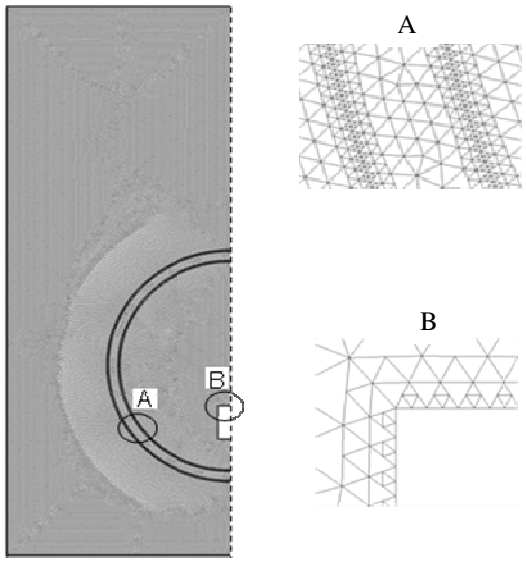

Figure 3. Computational domain and typical discretization.

The balloon is located inside a cylindrical shield matching the dimensions of the experimental shield. No slip, isothermal boundary conditions are applied on the shield.

The axisymmetric computational domain and a typical mesh utilized in the numerical simulations are shown in Fig. 3. Note that the mesh is refined in the vicinity of the balloon boundaries. Following the study of Samanta et al [1] convergence of the buoyancy force was achieved when the total number of grid volumes was more than about 6×10^4. In all calculations that follow, we used grid containing about 7×10^4 volumes to obtain grid independent results. A number of computations were also performed on denser grids containing more than 10^5 volumes. The relative differences between the buoyancy force values obtained on denser and coarser grids were less than 1% verifying a grid independence of the results.

IV. Analytical Model

Following the previous work of Samanta et al[1] the buoyancy of the both single- and double-walled Titan Montgolfiere prototype can be estimated by applying external, gap and internal natural convection heat transfer correlations. In these estimates, the balloon is assumed spherical, and the presence of any external boundaries such as the shield in the experiments is neglected. The correlations determine a functional dependency of the *Ra* number with the corresponding *Nu* number defined as:

$$Ra = Pr g \Delta T L^3 \beta / \nu^2 , \qquad Nu = hL/k, \tag{6}$$

where L is a characteristic length related to external diameter, gap width or internal diameter of the balloon depending on a specific choice of the correlation. While the form of these correlations as a power law is suggested by boundary layer theory, in turbulent convection the constants must be determined empirically from laboratory tests. It should be noted that the correlations below are based on measurements made in canonical situations where the internal, gap, and external convection are considered independently on rigid, spherical specimens, and under

conditions where the surface temperature is held (approximately) uniform on all surfaces. While such correlations are often quite accurate for the exact configurations they are intended, a significant (and not easily quantified) uncertainty is introduced in using them for the present situation where both temperature and heat flux show considerable variation over the balloon skin.

Once correlations are selected, the equations may be solved iteratively to determine the average internal temperature (and consequently the buoyancy) as a function of the heat rate. The specific correlations chosen to represent the internal, gap, and external convection are discussed in the following.

Step 1 – External Convection and Radiation

The correlation proposed by Campo [5] and verified by Jones and Wu [6] is utilized for the external convection:

$$Nu_{D_o} = \begin{cases} 2 + 0.6Ra_{D_o}^{0.25} & Ra_{D_o} < 1.5 \times 10^8, \\ 0.1Ra_{D_o}^{0.34} & Ra_{D_o} \geq 1.5 \times 10^8, \end{cases} \tag{7}$$

where $Ra_{Do} = Prg(T_o - T_\infty)D_o^3\beta/\nu^2$. The obtained Nusselt number along with the known heat input $\dot{Q}$ are then used to calculate the average temperature value of the external balloon surface T_o as follows from the definition of Nu_{Do} and a steady state energy conservation equation,

$$\dot{Q} = h_{ext}A_{ext}(T_o - T_\infty) + \sigma(T_o^4 - T_\infty^4), \qquad Nu_{D_o} = h_{ext}D_o/k. \tag{8}$$

Here k is the heat conduction coefficient, A_{ext} is a surface area of the external balloon boundary and σ is a Stefan-Boltzman constant. Note that all physical properties of the flow (i.e. Pr, β, ν, k) are evaluated at an external film temperature, T_{of} as detailed in Table 2.

Step 2 – Convection and Radiation Inside the Spherical Gap

The next stage computes the average temperature of the internal balloon boundary, T_i, by utilizing the correlation of Scanlan et al [7] for heat transfer in the enclosure between two concentric spheres

$$\dot{Q} = Nu_g 4\pi k(T_i - T_o)R_i^2/L + \dot{Q}_{rad}, \quad Nu_g = 0.228\left(Ra_g\,(1-\phi)/\phi\right)^{0.226}/\phi. \tag{9}$$

Here $\phi = R_i/R_o$ ratio and the heat lost due to radiation effects is defined as in [8] by:

$$\dot{Q}_{rad} = \sigma A_i(T_i^4 - T_o^4)/\left(\frac{1}{\varepsilon_1} + \frac{1-\varepsilon_2}{\varepsilon_2}\phi^2\right), \tag{10}$$

where ε_1 and ε_2 are the emissivity values of the internal and external sphere surfaces and A_i is a surface area of the internal surface. In this case all physical properties of the flow are taken at a gap film temperature T_{gf} (see Table 2 for details).

Step 3 – Internal convection

The average temperature of the internal balloon boundary, T_i, calculated in step 2, is then used to determine the average temperature of the balloon interior T_b. For this purpose the correlation of Carlson and Horn [9] is used

$$Nu_{D_i} = \begin{cases} 2.5\left(2 + 0.6Ra_{D_i}^{0.25}\right) & Ra_{D_i} < 1.35 \times 10^8, \\ 0.325Ra_{D_i}^{0.333} & Ra_{D_i} \geq 1.35 \times 10^8, \end{cases} \tag{11}$$

where $Ra_{Di} = Prg(T_b - T_i)D_i^3\beta/\nu^2$. Similarly to the external convection case

$$\dot{Q} = h_{int}A_{int}(T_b - T_i) + \sigma(T_b^4 - T_i^4), \qquad Nu_{D_i} = h_{int}D/k. \tag{12}$$

In this case all physical properties of nitrogen are taken at the interior film temperature T_{if} as defined in Table 2.

Table 2. Formulas for computation of average temperature values.

Media Boundaries and Temperatures		Average Temperature Value
External sphere boundary Infinity	T_o T_∞	$T_{of} = (T_o + T_\infty)/2$
Internal Sphere boundary External Sphere boundary	T_i T_o	$T_{gf} = \dfrac{(\bar{R}^3 - R_i^3)T_i + (R_o^3 - \bar{R}^3)T_o}{R_o^3 - R_i^3}, \bar{R} = \dfrac{(R_o + R_i)}{2}$
Internal Sphere Media Internal Sphere boundary	T_b T_i	$T_{if} = (T_i + T_b)/2$

As in the simulations, the nitrogen density ρ was calculated by using the ideal gas law while Sutherland's law was used to calculate the dynamic viscosity μ, and thermal conductivity k at different temperatures. Tabulated values were used to find the specific heat c_p. The average density values of the internal sphere and the gap determine the overall balloon buoyancy,

$$B = \frac{\pi}{6}g\left(D_i^3(\rho_g - \rho_b) + D_o^3(\rho_\infty - \rho_g)\right). \tag{13}$$

Note that in order to predict the buoyancy of a single-walled balloon we use only steps 1 and 3 whereas $T_o \equiv T_i \equiv T_g$. The above approach does not include an explicit modeling of the heat source whose thermal radiation heat transfer is predicted on the basis of the balloon interior averaged temperature T_b. Therefore we expect that the engineering correlations underestimate the realistic radiation effect. A more precise estimation of the thermal radiation effect would be obtained by an explicit modeling of the heat source implemented in our numerical model and discussed in the following section.

V. Results and Discussion

A. Qualitative flow features

The CFD model calculates the time-averaged temperature and flow fields for the balloons in a cryogenic environment. The results of the temperature distribution and streamfunction for the single- and double-walled balloons are shown in Figs. 4-a and 4-b respectively. The ambient temperature used in the simulation shown in Fig. 4 was T_∞ = 90K, and the heat input was $\dot{Q} = 550\ W$. The typical internal flow structure is characterized by

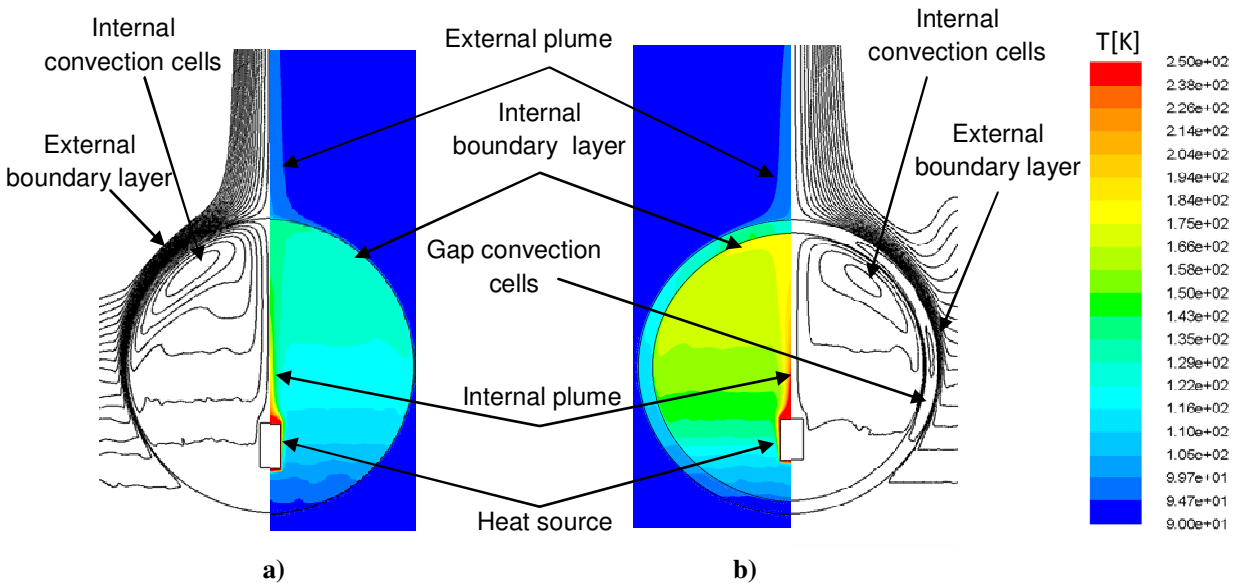

Figure 4. Temperature and stream function distributions inside: a) single-walled balloon; b) double-walled balloon. T_∞=90K, $\dot{Q}$ =550 W.

plumes, convection cells, and (momentum and thermal) boundary layers. An internal plume is formed adjacent to a heating element and rises along the centerline of the balloon, and an external plume is formed above the crown. In this time-averaged turbulent flow, a single recirculating convection cell (of toroidal shape) forms within the inner sphere. The recirculation is more intense (faster) at the top. One can also distinguish the existence of a cell in the gap for the double-walled case (see Fig. 4-b). Both single- and double-walled balloons are predicted to have very thin momentum and thermal boundary layers close to the surfaces. These are evidenced by the nearly discontinuous temperature field adjacent to the surfaces. The largest convective velocities occur where the streamlines are closest together; this occurs on both internal and external surfaces adjacent to the intense part of the internal convection cell.

As expected, and as can also be seen from Fig. 4, the insulating effect of the gap leads to a higher average temperature in the double-walled balloon than in the single-walled one when the heat input for both balloons is the same.

B. Single-walled balloon buoyancy

Figure 5 presents a comparison between experimental, numerical and correlation values of the single-walled balloon buoyancy. In these comparisons, radiation heat transfer is switched off. Error bars on experimental data represent $\pm 3\sigma$ limits, where σ is the standard deviation of the load cell data. There is good agreement between the numerical and experimental results for the entire range of ambient temperatures and heat inputs. Discrepancy between the results is larger for higher heat transfer rates between the balloon and the surroundings. The discrepancy increases as the ambient temperature decreases and reaches its maximum (about 10%) at T_∞=90K. The same trend is observed for the results obtained by using empirical correlations (7) and (11) which in general underestimate the buoyancy. The maximal discrepancy between the correlated and numerical buoyancy values is about 20% when

$\dot{Q} = 550W$ and T_∞ = 90K. Note that underestimated buoyancy values obtained with empirical correlations for a single-walled balloon were also observed by Samanta et al [1]. Finally, we note that accounting for the 3% and 7% smaller surface area and volume, respectively, of the experimental balloon compared to the simulated one would result in a better match of the computational data, but a greater discrepancy with the correlation.

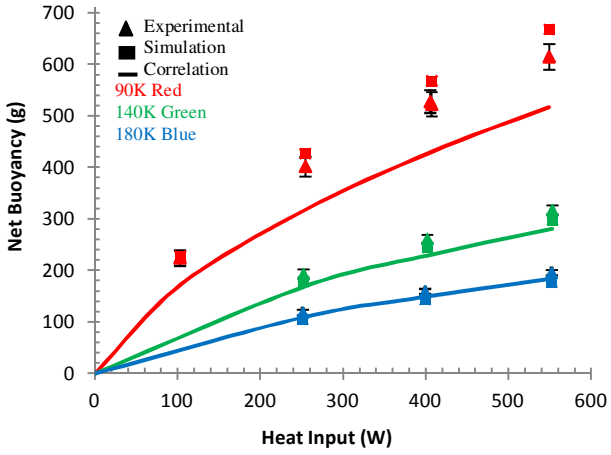

Figure 5. Net buoyancy of the single-walled 1m balloon.

C. Double-walled balloon buoyancy

As has been already mentioned, the doubled wall balloon is characterized by a superior thermal efficiency due to insulating effect of the gap between internal and external spheres. In fact for the entire range of the ambient temperatures and heat inputs the buoyancy of the doubled-wall balloon is at least 25% more than that obtained for the corresponding configuration of a single-walled balloon. This observation is correct either for numerical and correlated or experimentally obtained buoyancy values (see Figs. 5 and 6). As for the case of a single-walled balloon error bars on experimental graphs represent $\pm 3\sigma$ were once again σ is a standard deviation obtained basing on the load cell measurements. Note that the values of σ in the experimental data of doubled-wall balloon are much smaller than those for a single-walled one. This may be a result of an insulating effect of the gap resulting in higher and more evenly distributed temperature inside the balloon and by this means stabilizing the internal convective flow. Similar to the single-walled balloon configuration there is a good agreement between numerical and experimental values of buoyancy obtained for the doubled-wall balloon. The deviations between the two values increase with the heat input reaching their maximum of about 10% at T_∞= 90K and $\dot{Q} = 700W$. This is in contrast with the results obtained using empirical correlations, which overestimate the buoyancy values of the double-walled balloon by as much as 30%. In order to account for the 15% smaller volume of the actual experimental balloon compared to the 1 m sphere, we recomputed the correlations using an effective spherical diameter of 0.95 m (again with ϕ= 0.9), the results of which are shown by the dashed line Figure 6. While this brings the correlation closer to the data, there remains a 20% over-prediction, which is especially troubling in light of the under-prediction of the single-walled results. Clearly there must be an over-prediction of the insulating properties of the gap inherent in equation (9).

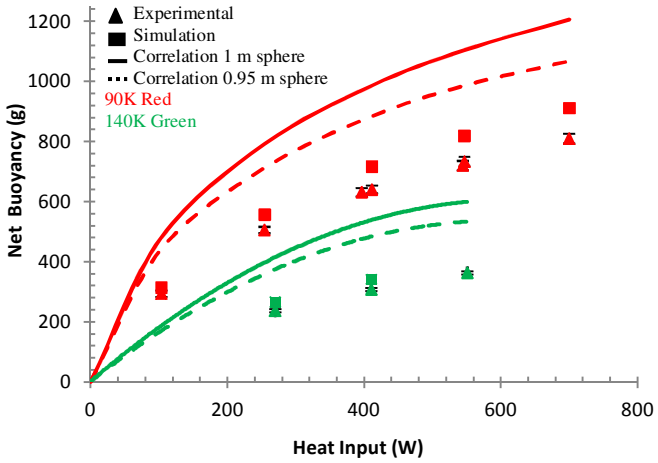

Figure 6. Net buoyancy of the double-walled 1m balloon.

In order to investigate the gap correlation, we use the simulation results to evaluate the local values of temperature and heat flux at each point on both surfaces. These values are then averaged over the surfaces and converted to non-dimensional values of Nusselt and Rayleigh numbers. The results are shown in Fig 7. Also plotted is the gap correlation due to Scanlan [7] (Eq. 9), which is based on measurements of the gap between two spheres heated to uniform temperature. It can be seen that for a scaled balloon experiments the correlation based on a uniform surface temperature yields considerable smaller values of the effective gap conductivity than the CFD results.[6] The lower conductivity values overestimate the insulating effect of the gap resulting in overpredicted buoyancy values. It should be noted however that the present simulations are restricted to $Ra^* < 7.3\times10^7$ which does not extend to the range of Ra^* expected for a full-scale Titan Montgolfiere. In addition, we also found (not shown

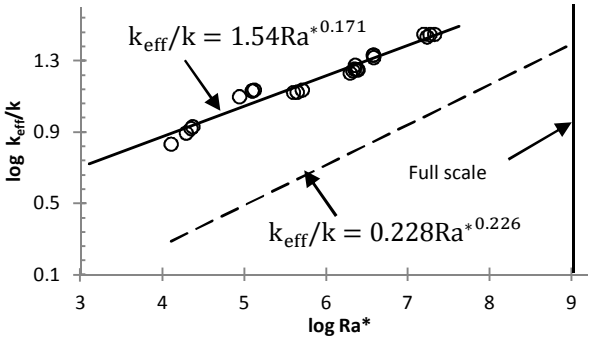

Figure 7. Correlations for convective heat transfer inside the spherical gap. The symbols correspond to the simulations of the different operating conditions and different values of ϕ. The solid line is the best fit of the data while the dashed line is the correlation of Scanlan (Eq.9).

[6] As an aside, it is interesting to note that the direct numerical simulations of Scurtu et al.[10] of the spherical gap with constant temperature surfaces at moderate Rayleigh numbers around 2×10^5 also show a 15% higher effective conductivity compared to the Scanlan correlation [7].

here) that this correlation is valid only for relatively narrow gaps ($\phi > 0.85$). This, however, is not likely to be a limitation for a realistic Titan Montgolfiere whose typical external diameter is about 10 m and gap width is characterized by $\phi > 0.85$ due to structural and other considerations. Simulations at full-scale conditions will be a focus of our future research.

Useful information can be extracted from numerical estimation of the net buoyancy as a function of heat input for different gap widths. As follows from Fig.8, the thermal efficiency of the doubled wall balloon increases with increasing a gap width to a maximum a ϕ =0.89. Further increase in gap width results in a slight decrease of the net buoyancy in agreement with the previous study of Samanta et al[1].

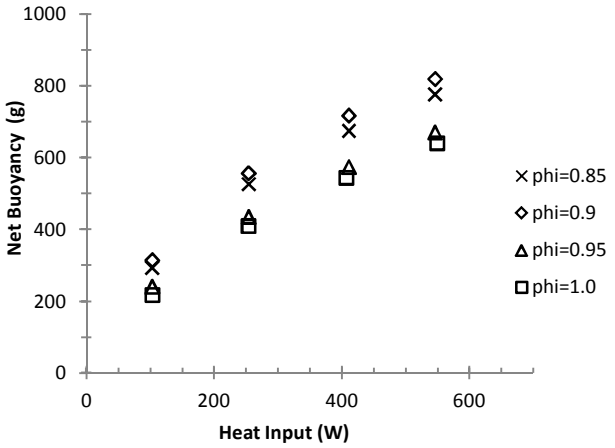

Figure 8. Net buoyancy versus heat input for different gap widths, 1 m external diameter balloon.

D. Radiation Effects

Radiation effects become significant when there is a large temperature difference between two or more surfaces or between surface and infinite surroundings participating in a heat transfer. For the idealized balloon with a spherical envelope, underlying the engineering correlations, the radiation loses from its surface to the surroundings are easily estimated and proportional to the difference in temperature to the fourth power. This approach however does not yield a precise estimation of the radiation interaction between the heat source and the inner surface of the balloon since the former is idealized as a constant thermal output with no physical surface. We thus expect an underestimation of the radiation heat transfer when using correlations.

For this reason the developed numerical model contains a physical heat source of cylindrical form (see Fig.3) whose height is the same with the heat source which was used in experiments. It should be noted however that the surface area of a real heat source is not cylindrical and contains numerous fins. Thus for the same heat power the surface temperature of the heating element in the numerical simulations is higher than in the real experiment, consequently overestimating radiation heat transfer between the heating element and the internal balloon skin.

For the present cryogenic operating conditions, our numerical calculations show that the radiation heat fluxes comprise at most few percent of the overall heat input. As can be seen from Fig. 9 considering the radiation leads to 1% and 5% decreases in buoyancy, respectively. Activation of the radiation model the double-walled balloon (not

shown) yields about the same small changes of net buoyancy values. We note in passing that the addition of the radiation model brings the simulations and experiments into closer agreement, but, especially given the relatively small effect of radiation, the difference is probably within the uncertainty associated with the turbulence modeling and other idealizations.

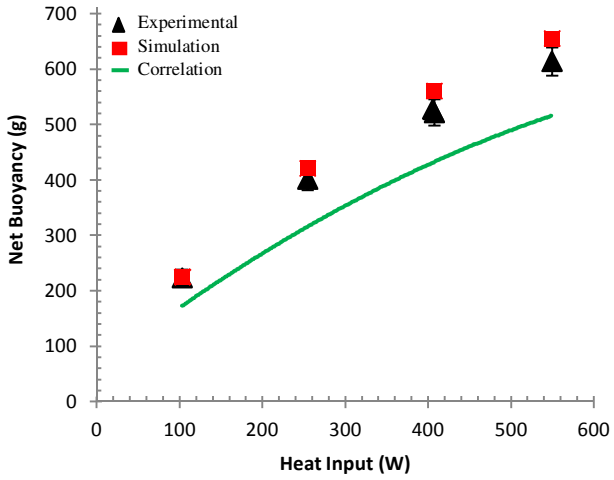

Figure 9. Net buoyancy versus heat input with radiation included, single-walled 1 m balloon, T_∞ = 90K.

For the present cryogenic operating conditions, our numerical calculations show that the radiation heat fluxes comprise at most few percent of the overall heat input. As can be seen from Fig. 9 considering the radiation leads to 1% and 5% decreases in buoyancy, respectively. Activation of the radiation model the double-walled balloon (not shown) yields about the same small changes of net buoyancy values. We note in passing that the addition of the radiation model brings the simulations and experiments into closer agreement, but, especially given the relatively small effect of radiation, the difference is probably within the uncertainty associated with the turbulence modeling and other idealizations.

E. Local Temperature Distribution

We now compare the individual temperatures recorded at 27 and 31 thermocouples distributed throughout the gas and balloon/shield surfaces, for the single- and double-walled balloon, respectively. Thermocouples were placed in a single plane through vertical centerline of the balloon at locations shown in Fig. 10. To quantify the differences between the experiments and simulations, we define the deviation between the measurements by

$$\xi = \left(T_{sim} - T_{exp}\right)/(T_{25} - T_\infty). \tag{14}$$

We note that we normalize the deviation by the temperature at thermocouple #25 relative to ambient temperature. We used this normalization since thermocouple #25 generally gives the highest temperature of all thermocouples, with the exception of the one mounted adjacent to the heater. This provides a fair comparison of the relative differences seen across all thermocouple positions. Deviation defined with respect to each individual thermocouple show larger values for those thermocouples reading close to ambient temperature. However, as the experimental ambient temperature was not held precisely constant during the experiment, we believe defining deviations with respect to the maximum temperature difference across the thermocouples gives rise to simpler interpretation of the

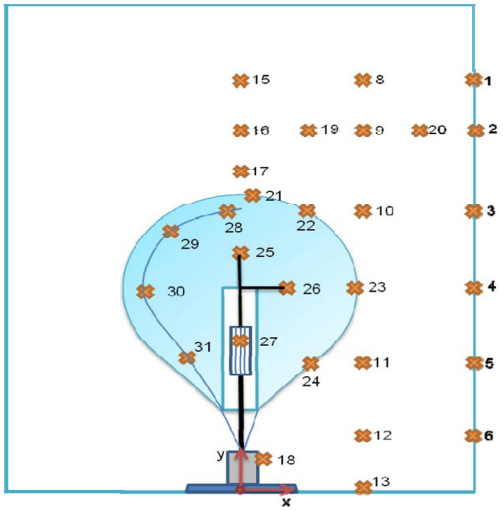

Figure 10. A schematic of the thermocouple locations in a single- and double-walled balloon.

data. Thermocouples accuracy is estimated as ±1K, and is not expected to introduce significant uncertainties in the following comparisons.

The comparisons are shown in Figure 11 for the operating points where ambient temperature was 90 K. Generally, deviations for the other ambient temperatures were smaller than those at 90 K, but lead to similar overall conclusions. In the figure, we have grouped thermocouples by balloon type (single or double), heat input, and whether the thermocouple was position in the gas or on the surface of the balloon.

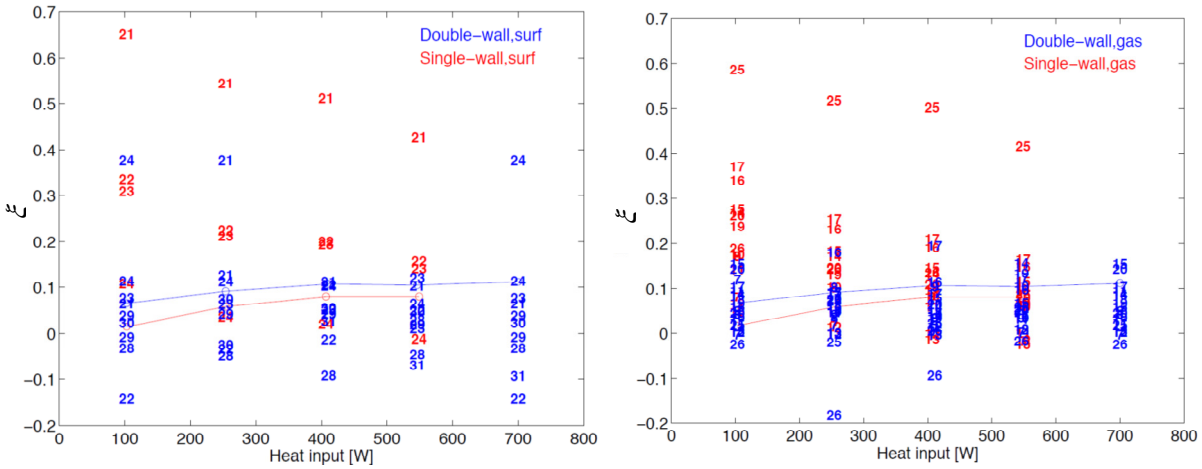

Figure 11. Relative temperature deviation between numerical and experimental local temperatures.

The majority of cases show deviations between experiment and simulation between about -5% and +15%. These temperature deviations are somewhat larger than those in net buoyancy, which are superposed on the plots (solid lines). For all values of heat input, the simulated balloon is generally hotter than the corresponding experiment, so it is expected that corresponding thermocouple deviations will mostly be positive. It is also reasonable to expect a

larger scatter in the deviation of the pointwise temperature field than in the net buoyancy, since the latter is approximately proportional to the balloon-volume-averaged temperature difference with ambient.

Regarding larger deviations between experiment and simulations, some trends are evident in the plots. The scatter is generally reduced as the heat input is increased, which is expected since corresponding difference with ambient temperature simultaneously becomes larger. We see the largest discrepancies occur for the single-walled balloon, but, for either case, significant positive deviations occur in the hot plume above the heat source (25), the balloon crown (21), and the hot plume above the balloon (17), and to a lesser extent at the other surface positions (22-24). Apparently the narrow plume above the heat source is significantly hotter in simulations than in experiments. We believe the discrepancy can be attributed to some unintended motion of the balloon which was evident in videos taken during the experiments. The motion was sufficiently slow such that it was not expected to result in any significant forced convection, but the consequent meandering of the thin plume emanating from the heater and balloon top may have caused thermocouples near the plume to be periodically exposed to the plume and to lower temperature fluid outside the plume. Likewise, turbulent convection in plumes tends also to be highly unsteady with large-scale instabilities (similar to those which are readily observed in the tip of a lit cigarette). One might expect that uncertainties in both the turbulence model to be largest at these locations. Given that the plume itself occupies a relatively small portion of the balloon volume, these larger deviations apparently do not translate into significant deviations in the net buoyancy.

Regarding the larger temperature deviations occurring at other surface positions, these may also indicate larger uncertainties in the turbulence modeling of the very thin, turbulent boundary layers. The boundary layers are predicted using a standard "wall model", which does not resolve the inner details of the turbulent boundary layer. Correspondingly, there are relatively large temperature gradients across computational cells comprising the boundary.

Significant negative deviations are seen for the double-walled balloon at thermocouple position 26 (off-axis above heat source in balloon) and 22 (outer surface midway between equator and crown). Given the opposite trend in the nearby plume/centerline, this tends to indicate that heat is distributed somewhat more evenly in the experimental flow than in the simulated one.

Again, for most thermocouples, the comparison between experiment and simulation obtained from the thermocouple data shows deviations in the range of ± 5-10%. These deviations may indicate a larger uncertainty in the numerical simulations, and especially parameters associated with the turbulence model, than we would infer from the relatively better agreement in the net buoyancy.

F. Universal Buoyancy Scaling

When the temperature difference between the internal gas and ambient conditions is sufficiently small, the strong Boussinesq approximation (see the discussion in section III) may be employed and, in this case, a dimensional analysis [1] shows that there exists, in the absence of radiation, a universal relation between a non-dimensional buoyancy, $b = (6B)/(\pi\rho_\infty v_\infty^2)$, and a non-dimensional heat input, $q = \left(gD^2\dot{Q}\right)/\left(\rho c_p T_\infty v_\infty^3\right)$ for single-walled balloons. At higher temperature differences, the universal scaling is not achieved, and the non-dimensional buoyancy would also depend on the specific variations of density and other fluid properties with temperature (and

thus on the ambient temperature value). In addition, radiation losses become increasingly important for larger temperature differences. It should be noted that for full-scale Titan balloon, the temperature differences from ambient are expected to be quite small and the universal scaling is expected to be closely followed. Even for smaller scale balloons, the scaling still provides a useful way to compare buoyancy data for a wide range of balloon sizes and heat inputs.

In Fig. 12, we present the CFD and experimental data from the present study along with the values from our previous simulations and experiments in the Titan Sky Simulator [1]. There is a reasonable collapse of all the data, and, again, the discrepancies between the previous and current simulations is due to relaxation of the strong Boussinesq approximation and the insertion of temperature-dependent properties in the current work. One notices some departures from non-universality in the small-scale experimental and simulation data, where three groups of points with slightly different slopes and y-intercepts. These groups correspond to the different values of T_∞.

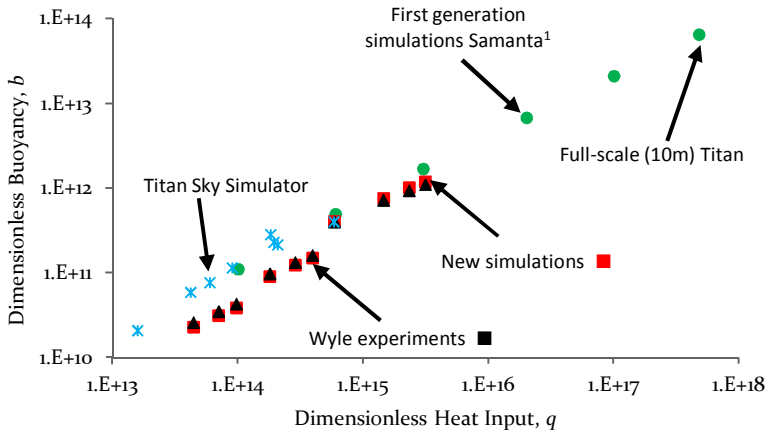

Figure 12. Dimensionless buoyancy against dimensionless power input for different experimental and numerical data.

The discrepancies between the previous and current experiments remain unexplained. We note that in the corresponding plot in our previous paper[1] constant fluid properties (evaluated at 103K) were used to scale the Titan Sky Simulator data for comparison with the simulations; the present plot uses the actual fluid properties at the ambient temperature corresponding to each experimental point, so the apparent discrepancies between the two sets of experimental data reflect actual differences in the (dimensional) buoyancy for a particular value of heat input and ambient temperature.

If a dependable correlation for the insulating properties of the gap of the double-walled balloon can be obtained, then a similar universal relationship would hold for each value of ϕ. In our future simulations, we will examine larger-scale, modest heat input cases in order to confirm these scaling trends for application to the full-scale Titan Montgolfiere.

VI. Conclusions

We reported on a computational and experimental study aimed at prediction of buoyancy and temperature field of the scaled Titan Montgolfiere at terrestrial, cryogenic conditions. The numerical solutions computed by a standard

k-ε turbulence model for an idealized spherical single- and double-walled balloon compare favorably with the corresponding results obtained experimentally. The maximum difference in net buoyancy between numerical and experimental results for both configurations is about +10%. Individual thermocouple measurements typically showed deviations, relative to the maximum temperature difference with ambient measured in each case, in the range of -5% to +15%. Larger deviations, especially for the single-walled balloons, were observed in the narrow turbulent plumes above the heater and above the balloon, and on adjacent surfaces. For the cryogenic conditions considered here, thermal radiation effects were found to have minimal effect on the net buoyancy. Overall, the simulations thus appear to be reliable for quantitative prediction of the temperature field and net buoyancy to within uncertainties associated with turbulence modeling. Future simulations with the detailed balloon geometry, and corresponding experiments at larger-scale will permit a more detailed understanding of scaling effects and modeling accuracy for the full-scale Titan Montgolfiere.

Engineering correlation models for the net buoyancy were also compared with experiment and simulation. For single-walled balloons these underestimate the buoyancy by as much as 20%, while for the double-walled balloons, they overestimate the buoyancy by as much as 30%. The latter is a more significant issue, since the insulating effect of the gap is a critical design feature ensuring feasibility of the Titan Montgolfiere. In the model-scale results here, the double-walled balloon is characterized by about 25% than a single-walled one, and it was found that a gap width is characterized by the value of $\phi = 0.9$ (which corresponded to the experimental specimen) was nearly optimal for the present operating conditions. The simulation data implies that the engineering correlation underestimates the effective conductivity of the gap, and is the primary source of the overall correlation's over-prediction of the double-walled balloon buoyancy. Spatial nonuniformity of the temperature and heat flux along the balloon surfaces is the likely culprit for the apparent failure of the gap correlation. The possibility of using simulation to provide a more accurate gap convection correlation will be investigated in future.

Acknowledgments

Part of this research was carried out at the Jet Propulsion Laboratory, California Institute of Technology, under a contract with the National Aeronautics and Space Administration. The help and support of the engineering and technical staff of Wyle Labs in El Segundo and their cryogenic chamber facility during the experiment is greatly acknowledged.

References

[1] Samanta, A., Appelo, D., Colonius, T., Nott, J., Hall, J., "Computational Modeling and Experiments of Natural Convection for a Titan Montolfiere," *AIAA Journal*, Vol. 48, No. 5, 2010, pp. 1007-1016.

[2] Dorrington, G. E., "Planetary Flight Surge Faces Budget Realities," *Advances in Space Research*, Vol. 47, No. 1, 2011, pp. 1-19.

[3] Nott, J., and Rand, J., "The Titan Sky Simulator™ Test Facility," AIAA Balloon System Conference, AIAA Paper 2007-2625, Williamsburg, VA, May 2007.

[4] Launder, B. E. and Spalding, D. B., *Lectures in Mathematical Models of Turbulence,* Academic Press, London, 1972.

[5] Campo, A., "Correlation Equation for Laminar and Turbulent Natural Convections from Spheres," *Wärme- und Stoffübertragung,* Vol. 43, Nos. 1-2, 1980, pp. 93-96.

[6] Jones, J., Wu, J.-J., "Performance Model for Reversible Fluid Balloons," AIAA Paper 95-1608-CP, 1995.

[7] Scanlan, J. A., Bishop, E. H., and Powe, R. E., "Natural Convection Heat Transfer Between Concentric Spheres," *Int.J. Heat Mass Transfer*, Vol. 13, 1970, No. 12, pp. 1857-1872.

[8] Incropera, F. P. De Witt, D. P., *Introduction toHeat Transfer,* Wiley & Sons, New York, 1985.

[9] Carlson, L. A., and Horn, W. J., "New Thermal and Trajectory Model for High Altitude Balloons," *Journal of Aircraft*, Vol. 20, No. 6, 1983, pp. 500-507.

[10] Scurtu, N., Futterer B., and Egbers, C., "Three-dimensional natural convection in spherical annuli," *Journal Phys.: Conf.Ser.*, Vol. 137, 012017, 2008.